

## Photodissociation spectroscopy via a rovibrational resonance in intense UV pulses

Yan Rong Liu<sup>1</sup>, Victor Kimberg<sup>2</sup>, Yong Wu<sup>3,4</sup>, Jian Guo Wang<sup>3</sup>, Oriol Vendrell<sup>5</sup>, and Song Bin Zhang<sup>1,\*</sup>

<sup>1</sup>*School of Physics and Information Technology, Shaanxi Normal University, Xi'an 710119, China*

<sup>2</sup>*Department of Chemistry, KTH Royal Institute of Technology, 10691 Stockholm, Sweden*

<sup>3</sup>*Institute of Applied Physics and Computational Mathematics, Beijing 100088, China*

<sup>4</sup>*Center for Applied Physics and Technology, Peking University, Beijing 100084, China*

<sup>5</sup>*Theoretical Chemistry, Institute of Physical Chemistry, Heidelberg University, 69120 Heidelberg, Germany*



(Received 12 July 2022; accepted 8 September 2022; published 3 October 2022)

Photodissociation dynamics via a rovibrational resonance in intense UV pulses is investigated theoretically, using a showcase  $\text{CH}^+$  molecule promoted to the  $\text{C } ^1\Sigma^+$  valence excited electronic state with a potential barrier, thus giving access to study shape resonance controlled by the pulse frequency. Simulations of the kinetic energy release (KER) and angular distribution of the photofragments (ADP) spectra show dramatic differences for the cases when the pulse is tuned on and off the rovibrational resonance. It shows that as the increasing pulse intensity for the transitions to shape resonance, the KER spectra develop into new and higher energy peaks overlying on the broadened background, which is explained by the involvement of other resonances with higher partial waves through electronic Rabi flopping between the ground and excited electronic states. Those nonlinear contribution increases drastically the probability of photofragmentation along the laser polarization in the ADP spectra. The coincident KER-ADP spectra reveal clearly the correlated dynamics in the vicinity of the dissociation barrier. The present work opens possibilities for the manipulation of ultrafast photodissociation dynamics with the help of resonance states in the continuum.

DOI: [10.1103/PhysRevResearch.4.043001](https://doi.org/10.1103/PhysRevResearch.4.043001)

### I. INTRODUCTION

Numerous light-induced ultrafast processes in atoms and molecules have been revealed and investigated [1–7], with the development of ultrashort and intense high-frequency laser sources [8–15]. In that context, photodissociation has attracted a broad interest in the past years due to versatile applications in UV and soft x-ray range [6,16–18]. To mention a few: the highly spin-polarized deuterium source can be obtained via the photodissociation of deuterium iodide [19]; the spontaneous relaxation of  $\text{CH}^+$  to its lowest rotational states can be monitored by studying photodissociation of an internally cold beam of  $\text{CH}^+$  ions in a cryogenic storage ring [20]; the control of ultracold photodissociation with magnetic fields shows that ultracold molecule techniques allow a high level of control over basic chemical reactions with weak applied fields [21]; and crossed beam photodissociation imaging of  $\text{HeH}^+$  with vacuum ultraviolet free-electron laser pulses shows that the photodissociation perpendicular to the laser polarization has a clear dominance [22].

Resonant excitation plays an important role in diverse dynamic processes. For example, an asymmetric time delay

was observed originating from the interference between resonant and nonresonant photoionization pathways [23]; the photoassociation rates can be enhanced by several orders of magnitude by nonresonant-light control of shape resonances [24]; the Rabi oscillations with long decay time between an atom pair and a molecule in an optical lattice were observed as a result of extremely small transition rate that is overcome by enhanced Franck-Condon factor of a weakly bound Feshbach molecule [25]; the electron-scattering dynamics dominated by a shape resonance shifted to lower energies due to molecular bond stretches during the evolution of a vibrational wave packet [26]; the molecular-frame anisotropies of the photorecombination amplitudes and phases caused by a shape resonance have also been revealed [27].

In previous studies devoted to photodissociation dynamics, the effect of electron-rotation coupling ( $\mathbf{R}-\Omega$  coupling) in diatomics by intense UV and x-ray pulses have been deeply investigated [28–32]. In particular, the effect of light-induced conical intersection on the photodissociation dynamics of the  $D_2^+$  molecule have been discussed [33–36], the effect of the lowest-lying  $\Pi$  electronic state in the photodissociation dynamics of LiF have been analyzed [37,38]; carrier-envelope phase effect of a sub-cycle UV pulse on the asymmetry of angular photofragments has also been revealed [39]. There is also an amount of work discussing the importance of resonances in molecular photodissociation, the van der Waals complex dissociation is analyzed based on the concept of resonance [40]; the photodissociation spectrum and the energy distribution of the photofragments is explained in terms of the shape resonances [41]; the electronic Feshbach resonance

\*song-bin.zhang@snnu.edu.cn

Published by the American Physical Society under the terms of the [Creative Commons Attribution 4.0 International license](https://creativecommons.org/licenses/by/4.0/). Further distribution of this work must maintain attribution to the author(s) and the published article's title, journal citation, and DOI.

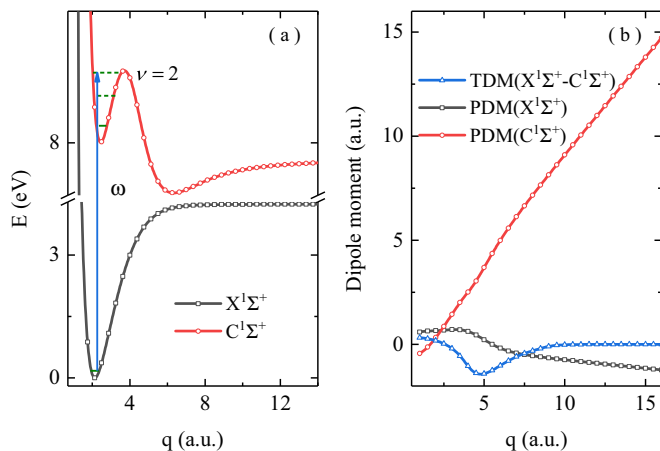


FIG. 1. (a) Potential energy curves (PECs) of  $\text{CH}^+$  for the ground  $X^1\Sigma^+$  and first valence excited  $C^1\Sigma^+$  electronic states; (b) the permanent dipole moments (PDM) and the transition dipole moments (TDM) for the two electronic states (data are reproduced from Ref. [46]). The strong UV pulse with  $\omega = 8.25$  eV is tuned into the resonance with  $\nu = 2$  vibrational level leading to direct fragmentation, and another case with  $\omega = 8.53$  eV above the potential barrier is studied for comparison.

and the existence of negative binding-energy states in neutral atoms is observed in soft x-ray-induced  $\text{O}_2$  dissociation [42]. However, there are not too many studies on photodissociation via resonances by intense pulses. It was shown that molecular photodissociation can be controlled through intense field zero-width resonances [43], the resonance coalescence in photodissociation provides a way to transfer completely the nondissociated molecules from one vibronic state to another [44].

In the present work, we study photodissociation dynamics in the vicinity of a rovibrational resonance state by intense UV pulses. We consider diatomic  $\text{CH}^+$  molecule as a showcase, excited from its ground  $X^1\Sigma^+$  to first valence-excited dissociative state  $C^1\Sigma^+$  with a potential barrier (more than 1.3 eV below state  $3^1\Sigma^+$ ), which has been well studied to support shape resonances [45,46]. Figure 1 illustrates the transition scheme, involved potential energy curves (PECs), as well as the dipole moments of the molecule. The PEC of the dissociative state  $C^1\Sigma^+$  shows two minima that are located at about 2.4 a.u. and 6.4 a.u. [46], the three vibrational levels or shape resonances of the first potential well are displayed in Fig. 1(a). The resonant UV pulse with  $\omega = 8.25$  eV promotes  $\text{CH}^+$  from its ground state  $X^1\Sigma^+$  to the rovibrational resonance state  $\nu = 2$  of state  $C^1\Sigma^+$ , triggering the molecular dissociation, as the lifetime for this resonance state is just about 81 fs [46]. Contrast to the resonance excitation, a nonresonant UV pulse with  $\omega = 8.53$  eV promoting molecule directly to a dissociative continuum is also studied for comparison. Kinetic energy release (KER) and angular distribution of the photofragments (ADP) spectra, as well as the coincidence KER-ADP map are detected to display information of the dissociation dynamics. We show that with an increase of the pulse intensity, additional resonance peak appears overlapping on the broadened KER spectra, and the intensity of ADP increases around  $\beta = 0$  or along the laser field polarization vector. As we will show, the

observed intensity dependence of the KER and ADP spectra can be explained by contribution from higher partial waves involved through electronic Rabi flopping between the electronic states  $X^1\Sigma^+$  and  $C^1\Sigma^+$ .

The paper is organized as follows. Theoretical approach to photodissociation dynamics in intense UV pulses is introduced briefly in Sec. II. Section III is devoted to the discussions of the KER, ADP, and the coincident KER-ADP spectra. Conclusions are given in Sec. IV. Atomic units (a.u.) are used through the whole paper if otherwise not stated explicitly.

## II. COMPUTATIONAL METHODS

Photodissociation of  $\text{CH}^+$  molecule by a linearly polarized laser field  $\varepsilon(\omega, t)$  with polarization along space-fixed  $Z$  axis could be described by the following nuclear Hamiltonian:

$$\mathbf{H}(\mathbf{q}, t) = [T_v(q) + T_{\mathbf{R}}(\mathbf{q})] + \begin{pmatrix} V_X(q) & 0 \\ 0 & V_C(q) \end{pmatrix} + \begin{pmatrix} T_{XX}(q, t) & T_{XC}^\dagger(q, t) \\ T_{XC}(q, t) & T_{CC}(q, t) \end{pmatrix}. \quad (1)$$

The first term includes the vibrational  $T_v = -\frac{\partial^2}{2m_\mu \partial q^2}$  and rotational  $T_{\mathbf{R}} = \frac{\mathbf{R}^2}{2m_\mu q^2}$  kinetic operators, where  $m_\mu$  is the reduced mass of  $\text{CH}^+$  molecule,  $q$  is the internuclear distance,  $\mathbf{R}$  is the nuclear rotational angular momentum and  $\mathbf{R}^2 = \mathbf{J}^2 - \Omega^2$ , with  $\mathbf{J}$  and  $\Omega = \Lambda + \Sigma$  are the total angular momentum and the total interior angular momentum about the molecular-fixed  $z$  axis, respectively, and  $\Lambda$  and  $\Sigma$  are the projections of the total orbital angular momentum  $\mathbf{L}$  and spin  $\mathbf{S}$  onto the molecular-fixed  $z$  axis [47]. For singlet state  $^1\Sigma$ ,  $\Lambda = \Sigma = 0$  and  $\mathbf{R}^2 = \mathbf{J}^2$ . In the second term,  $V_X(q)$  and  $V_C(q)$  correspond to the potential energy curves of states  $X^1\Sigma^+$  and  $C^1\Sigma^+$ , respectively [Fig. 1(a)]. Note that the resonant excitation dominates the loss of dissociative state to higher electronic states by sequential multiphoton excitation/ionization, higher electronic states are supposed to minorly reduce the total dissociation dynamics and not included [33–36]. The laser-molecule dipole interaction is described in the third term, where  $T_{ij}(q, t) = \mu_{ij}(q)\varepsilon(\omega, t)\cos\beta$  with  $\mu_{ij}(q)$  being the (transition) dipole moment [Fig. 1(b)] between electronic states  $i$  and  $j$  ( $\{i, j\} = \{X, C\}$ ), and  $\beta$  is the angle between molecular  $z$  axis and laser polarization along  $Z$  axis. The UV pulse is modeled as  $\varepsilon(\omega, t) = g_0 g(t)\cos(\omega t)$ , with peak intensity  $I = |g_0|^2$  and  $\tau = 50$  fs Gaussian envelope  $g(t) = \exp(-t^2/\tau^2)$ .

Solution of the nonstationary Schrödinger equation with Hamiltonian (1) allows us to find time-dependent rovibrational wave packet  $|\Phi_C(t)\rangle$  in the excited dissociative state  $C^1\Sigma^+$ . The dissociation dynamics, as well as KER and ADP spectra can be then computed using complex absorbing potential (CAP) technique in the form of  $-iW(q) = -i\eta(q - q_c)^3\Theta(q - q_c)$ , where  $\eta$  is the CAP strength,  $q_c$  is the point where the CAP is switched on,  $\Theta$  is Heaviside's step function. The KER-ADP coincident spectra for dissociation

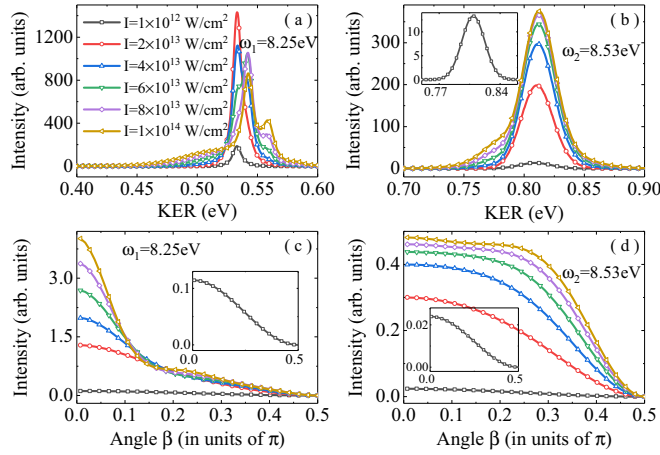


FIG. 2. (a), (b) KER spectra and (c), (d) ADP of the dissociation fragments from the  $C^1\Sigma^+$  state with the UV frequencies  $\omega = 8.25$  eV [(a), (c)] and  $\omega = 8.53$  eV [(b), (d)], respectively. The calculations are performed for six UV pulse intensities shown by different line colors and symbols [see the legends in (a)].

fragments in the upper state  $C^1\Sigma^+$  can be computed as [48]

$$P(\beta_j, E) = \frac{1}{w_j \pi} \int_0^\infty \int_0^\infty \langle \Phi_C(t) | W_{\beta_j} | \Phi_C(t') \rangle e^{-iE(t-t')} dt dt', \quad (2)$$

where  $w_j$  is the weight factor corresponding to the relevant grid point in the applied DVR basis,  $W_{\beta_j}$  is the projection of the CAP on a specific grid point associated with the rotational degree of freedom. Through integrating the kinetic energy or angle of  $P(\beta_j, E)$ , the one-dimensional ADP spectra and KER spectra can be achieved as  $P_{\text{angle}}(\beta_j) = \frac{1}{w_j} \int_0^\infty \langle \Phi_C(t) | W_{\beta_j} | \Phi_C(t) \rangle dt$  and  $P_{\text{KER}}(E) = \frac{1}{\pi} \int_0^\infty \int_0^\infty \langle \Phi_C(t) | W | \Phi_C(t') \rangle e^{-iE(t-t')} dt dt'$ , respectively. And total dissociation yield can be obtained through integration over all fragment energies and emission angles as  $P = \int_0^{2\pi} \int_0^\infty P(\beta_j, E) \sin \beta dE d\beta = \int_0^{2\pi} P_{\text{angle}}(\beta_j) \sin \beta d\beta = \int_0^\infty P_{\text{KER}}(E) dE$ .

The simulations are performed with the Heidelberg MCTDH package [48,49]. The vibrational degrees of freedom (DOF)  $q$  is described by sin-DVRs equally distributed ( $\Delta q = 0.1$  a.u.) in the region of [1.0–80.0] and [1.0–90.0] a.u. for resonance and nonresonance case; 101 basis functions have been used for the rotational DOF  $\beta$  by  $L^2$ -normalized Legendre polynomials  $P_J(\beta) = \sqrt{\frac{2J+1}{2} \frac{(J-M)!}{(J+M)!}} P_J^M(\cos \beta)$ , where  $P_J^M(\cos \beta)$  is the associated Legendre functions and  $M = 0$  in the present work. The number of single particle functions for both DOF on the two electronic states is 20, and the CAP is applied at the end of last 10 a.u. grid with  $\eta = 3 \times 10^{-5}$  a.u.

### III. RESULTS AND DISCUSSIONS

The cold ensemble is assumed that  $\text{CH}^+$  molecule is initially at  $\nu = 0$  and  $J_0 = 0$  of ground electronic state  $X^1\Sigma^+$ . Figure 2 shows the variations of KER and ADP spectra of dissociative state  $C^1\Sigma^+$  by different intense pulses, with  $\omega = 8.25$  eV resonant on the shape resonance  $\nu = 2$  of the

potential barrier [46], another case with nonresonant  $\omega = 8.53$  eV above the potential barrier is also studied for comparison. The KER spectrum consists of a single peak at around 0.533 eV by the low intense pulse ( $1 \times 10^{12}$  W/cm<sup>2</sup>) as shown in Fig. 2(a), corresponding to the resonant excitation to p-wave ( $J = 1$ ) resonance at  $\nu = 2$  level of the dissociative state  $C^1\Sigma^+$ ; while the KER spectrum for nonresonant excitation above the potential barrier [Fig. 2(b)] shows a peak at around 0.810 eV, with peak width determined by the bandwidth of pump pulse (about 0.05 eV). Increasing of pulse intensity results into the shift of resonance spectra towards higher KER and the formation of additional peaks at about 0.543 eV and 0.562 eV. Besides the varying of spectra intensity, a broad background is developed as the increasing of field intensity for nonresonant excitations [Figs. 2(a) and 2(c)], due to the broadening of energy levels dressed by intense field [28,29,50].

Since the pulse is shorter than the lifetime of p-wave rovibrational resonance (about 80 fs [46]), the selection rule  $\Delta J = \pm 1$  allows the excitation of higher odd waves of state  $C^1\Sigma^+$  by intense pulse through Rabi flopping between states  $X^1\Sigma^+$  and  $C^1\Sigma^+$ , resulting into the involvement and contribution of higher-wave (as  $J = 3, 5, \dots$ ) rovibrational resonances in the KER spectra, their energy levels relative to level  $\nu = 2$  of state  $C^1\Sigma^+$  are about  $J(J+1)/(2m_\mu q_{\nu=2}^2)$ , where  $q_{\nu=2}$  is the expectation value of  $q$  at  $\nu = 2$  of state  $C^1\Sigma^+$ . 0.543 eV and 0.562 eV are exactly the energy positions of rovibrational resonances  $J = 3$  and  $J = 5$  at  $\nu = 2$  of state  $C^1\Sigma^+$ . These resonance structures could be changed by more intense pulse from the light-induced potential.

Figures 2(c) and 2(d) present the ADP spectra for different pulse intensities. The ADP spectrum shows the typical  $\cos^2$ -like profile at weak intensity for the present  $\Sigma - \Sigma$  transition. With the increasing of pulse intensity, the ADP deviates sufficiently from the  $\cos^2$ -like profile; for dissociation via resonances, the fragments act more likely to release along the laser polarization ( $\beta \simeq 0$ ), and a limited plateau around  $\beta \simeq 0.25\pi$  is gradually built and becomes significant when the pulse intensity reaches  $1 \times 10^{14}$  W/cm<sup>2</sup>; while for the dissociation above potential barrier, a broad plateau starting from  $\beta \simeq 0$  is formed and gradually extended up to  $\beta \simeq 0.3\pi$  when  $I = 1 \times 10^{14}$  W/cm<sup>2</sup>, such a feature is consistent with the results revealed in previous work [28]. These features are related to different rotational excitations for different KER; in the following, the correlated dynamics of fragments with respect to KER and releasing angle are studied by coincident KER-ADP spectra.

Figure 3 shows the KER-ADP coincidence spectra by different intense pulses with central frequency via the shape resonance [Figs. 3(a), 3(c), and 3(e)], and above the potential barrier [Figs. 3(b), 3(d), and 3(f)]. As it clearly shows, with the increasing of pulse intensity, the coincident pattern via resonance develops into multippeak structures in both KER axis and angle axis [Figs. 3(a), 3(c), and 3(e)], mainly locating at  $\beta \simeq 0$ ; while the spectra by pulse above the potential barrier become broader in KER axis with peak pattern shifting to higher angle region [Figs. 3(b), 3(d), and 3(f)] from  $\beta \simeq 0$  to  $\beta \simeq 0.3\pi$ . Compared with the conventional one-dimensional angle-integrated KER and energy-integrated ADP shown in Fig. 2, the coincidence KER-ADP spectra provide more

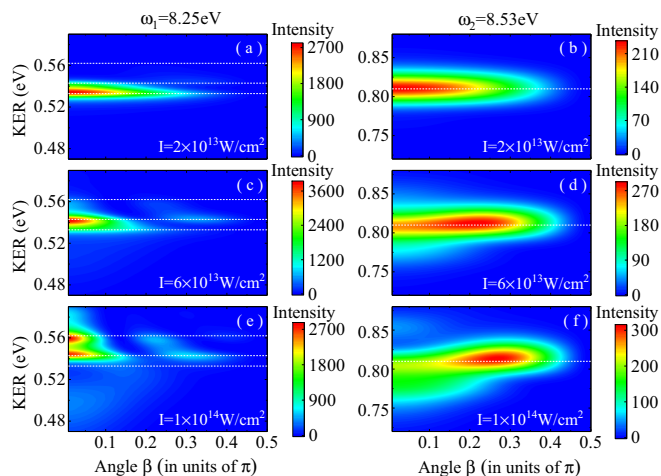


FIG. 3. Coincident KER-ADP spectra for (a), (c), (e) resonance excitation  $\omega = 8.25$  eV and (b), (d), (f) nonresonance excitation  $\omega = 8.53$  eV, with three pulse intensities  $2 \times 10^{13}$  W/cm $^2$  [(a), (b)],  $6 \times 10^{13}$  W/cm $^2$  [(c), (d)], and  $1 \times 10^{14}$  W/cm $^2$  [(e), (f)]. The dotted lines from bottom to top in (a), (c), (e) corresponding to the energy levels of rovibrational resonances pertaining to states  $J = 1, 3$ , and  $5$ , respectively; the dotted lines in (b), (d), (f) indicate the energy of direct stimulating.

details about the correlated dynamics and more degrees of freedom to investigate the nonlinear photodissociation process.

More detailed analysis for the structures shown in the correlation pattern are presented in Fig. 4 for intermediate intensity  $I = 8 \times 10^{13}$  W/cm $^2$ . As presented in Fig. 4(a), for dissociation via resonance, cases with KER = 0.533, 0.543, and 0.562 eV are selected [marked as  $E(J1)$ ,  $E(J3)$ , and  $E(J5)$ ], corresponding to the energy levels of rovibrational resonances pertaining to  $J = 1, 3$ , and  $5$ , respectively,

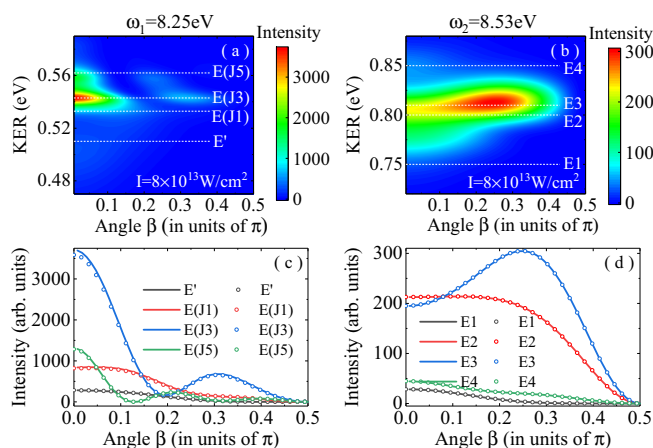


FIG. 4. Coincidence KER-ADP spectra for (a) resonance excitation  $\omega = 8.25$  eV and (b) nonresonance excitation  $\omega = 8.53$  eV with the UV pulse intensity  $I = 8 \times 10^{13}$  W/cm $^2$ . Correspondent ADP profiles [(c), (d)] for several fixed KER shown in (a) and (b), solid lines and dotted lines are the ADP obtained by coincidence spectra using using Eq. (2) and reconstructed ones using Eq. (4), respectively.

and the case of KER = 0.510 eV (marked as  $E'$ ) below resonance is also selected for comparison. For dissociation above potential barrier as shown in Fig. 4(b), cases with KER = 0.75, 0.80, 0.81, and 0.85 eV around the peak spectra are selected (marked as  $E1$ ,  $E2$ ,  $E3$ , and  $E4$ , respectively),  $E3$  locates exactly at the peak. The corresponding ADP spectra for these selected cases are shown as solid lines in Figs. 4(c) and 4(d). The spectra of  $E(J3)$  and  $E(J5)$  show one- and two-node structures, typical distributions for rotational states of  $J = 3$  and  $J = 5$ , respectively; the spectra of  $E2$  show an important plateau from  $\beta \simeq 0$  to  $\beta \simeq 0.2\pi$ , and the spectra of  $E3$  exhibit significant peak at about  $\beta \simeq 0.25\pi$ . These quite different features could be interpreted as the different interference results between the rotational states, based on the technique of constructing the spectra, as shown in Figs. 4(c) and 4(d) as the dotted lines.

The time-dependent rovibrational wave packet in dissociative state  $C^1\Sigma^+$  in a finite space after pump pulse can be expressed as

$$\Phi_C(q, \beta, t) = \sum_{J,E} C_J^E e^{-iEt} \varphi_J^E(q) P_J(\beta), \quad (3)$$

where  $t$  is the time with respect to pump pulse center,  $\varphi_J^E(q)$  and  $E$  are the vibrational eigenfunction and eigenvalue, respectively, for Hamiltonian  $H_J^C(q) = -\frac{\partial^2}{2m_\mu \partial q^2} + \frac{J(J+1)}{2m_\mu q^2} + V_C(q)$  (including centrifugal potential from total angular momentum  $J$ ),  $P_J(\beta)$  is the  $L^2$ -normalized Legendre polynomials (see last paragraph of Sec. II), the coefficient  $C_J^E$  can be calculated through projection as  $C_J^E = \langle \varphi_J^E(q) P_J(\beta) e^{-iEt} | \Phi_C(q, \beta, t) \rangle$ . The angular distribution at a specific energy  $E$  can be calculated at large time as  $P_{\text{angle}}^E(\beta) = \int |\Phi_C(q, \beta, t)|^2 dq = \int dq |\sum_J C_J^E \varphi_J^E(q) P_J(\beta)|^2$ . Since  $\varphi_J^E(q)$  is almost invariant for not highly excited  $J$ , we can reach the well-approximated relation as

$$P_{\text{angle}}^E(\beta) \simeq \left| \sum_J |C_J^E| e^{i\theta_J^E} P_J(\beta) \right|^2, \quad (4)$$

$\theta_J^E$  is the phase of different  $J$  state. Supposing the norm  $|C_{J=J_0}^E|$  dominates others, we can set  $\theta_{J=J_0}^E = 0$ , then  $\theta_J^E$  indicates the relative phase with respect to state  $J = J_0$ . As clearly presented in Figs. 4(c) and 4(d) the reconstructed spectra (dotted lines) using Eq. (4) agree well with the calculated ones (solid lines) using Eq. (2). Note that general agreements of dissociation above potential barrier are better than that of dissociation via resonance, it comes from the fact that, the resonance state with higher density of state is much more difficult to be mimicked with the same mesh grid and DVRs. The corresponding norm  $|C_J^E|$  and relative phase  $\theta_J^E$  for these spectra are collected in Table I.

As it follows from Table I, for cases of KER =  $E(J1)$ ,  $E(J3)$ , and  $E(J5)$  (where the rovibrational resonances locate), dominated higher rotational states are gradually excited through electronic Rabi flopping. Explicitly, when KER =  $E(J1)$ ,  $|C_1^E|$  is a little smaller than  $|C_3^E|$  (but much larger than others), states  $J = 1$  and  $J = 3$  superpose ‘in-phase’ ( $\theta_3^E$  in the right quadrant), resulting into the main structure of ‘monotonic’ decreasing with a slow decreasing

TABLE I. The parameters in the ADP profile at specific KER energies, where  $P_{\text{angle}}^E(\beta) \simeq |\sum_J |C_J^E| e^{i\theta_J^E} P_J(\beta)|^2$ ,  $|C_J^E|$  is the norm of  $P_J(\beta)$ , and  $\theta_J^E$  (in units of  $\pi$ ) is the relative phase.

	$E'$	$E(J1)$	$E(J3)$	$E(J5)$	$E1$	$E2$	$E3$	$E4$
$ C_1^E $	7.34	11.90	7.42	4.28	2.41	13.26	16.96	5.21
$ C_3^E $	6.47	15.46	29.06	3.43	1.47	7.85	8.50	0.83
$ C_5^E $	3.96	5.91	7.83	12.70	0.59	2.18	2.22	0.38
$ C_7^E $	1.49	2.08	2.25	2.46	0.18	0.45	0.44	0.17
$ C_9^E $	0.40	0.53	0.58	0.59	0.04	0.08	0.07	0.04
$ C_{11}^E $	0.08	0.11	0.12	0.12	0.01	0.01	0.01	0.01
$\theta_1^E$	0.00	-0.33	-0.63	0.60	0.00	0.00	0.00	0.00
$\theta_3^E$	0.30	0.00	0.00	-0.45	0.22	0.57	0.68	0.64
$\theta_5^E$	0.69	0.54	0.22	0.00	0.55	-0.80	-0.69	-0.29
$\theta_7^E$	-0.93	1.00	0.70	0.06	-0.98	-0.19	-0.09	0.15
$\theta_9^E$	-0.55	-0.63	-0.92	0.43	-0.47	0.38	0.47	0.63
$\theta_{11}^E$	-0.21	-0.28	-0.57	0.76	0.04	0.93	-0.99	-0.87

plateau at around  $\beta \simeq 0.35\pi$ , and the nonignorable contributions from ‘out-phase’ states  $J = 5$  and  $J = 7$  ( $\theta_J^E$  in the left quadrant) destruct the releasing probability at around  $\beta \simeq 0$ ;  $|C_3^E|$  (or  $|C_5^E|$ ) are much larger than others when KER =  $E(J3)$  ( $E(J5)$ ), resulting into its main structure following the distribution of state  $J = 3$  ( $J = 5$ ), the ‘in-phase’ state  $J = 5$  ( $J = 3$  and  $7$ ) increases the releasing probability along the laser polarization ( $\beta \simeq 0$ ), while the ‘out-phase’ states  $J = 1$  and  $J = 7$  ( $J = 1$ ) lift the node at about  $\beta \simeq 0.2\pi$  ( $\beta \simeq 0.3\pi$ ) and destruct the releasing probability at around  $\beta \simeq 0$ .

For other cases not via resonances, the coefficient  $|C_J^E|$  decreases as  $J$  increases. Cases of KER =  $E'$  and KER =  $E1$  are below the resonant frequency and show quite similar ‘monotonic’ decreasing spectra, mainly from the ‘in-phase’ interference between states  $J = 1$  and  $J = 3$ . When KER varies from  $E1$  to  $E4$ , to  $E2$  and to  $E3$  (closer to the peak position at KER =  $E3$ ), states  $J = 1$  and  $J = 3$  turn into ‘out-phase’ and the relative intensity of  $|C_3^E|$  increases, as shown in Table I. Since  $P_{J=1}(\beta)$  and  $P_{J=3}(\beta)$  evolve in-phase (out-phase) in the forward (backward) region, states  $J = 1$  and  $J = 3$  with ‘out-phase’ destruct and construct the probabilities when  $\beta < 0.5\pi$  and  $\beta > 0.5\pi$ , respectively, resulting into the

reducing and rising of probabilities at around  $\beta \simeq 0$  and  $\beta \simeq 0.25\pi$ , the nonignorable ‘out-phase’ state  $J = 5$  also destructs the releasing probability at around  $\beta \simeq 0$ . With the increasing of pulse intensity, the building of ‘out-phase’ higher rotational states and their superposition with  $J = 1$  contribute the shifting of peak pattern to higher angle region as shown in Figs. 3(b), 3(d), and 3(f), or the development of a plateau as shown in Fig. 2(d).

#### IV. CONCLUSION

In summary, the photodissociation dynamics induced by the intense UV pulse tuned to the rovibrational resonance  $\nu = 2$  of the dissociative state  $C^1\Sigma^+$  of  $\text{CH}^+$  molecules has been studied theoretically, nonresonant excitation case above the potential barrier is also studied for comparison. We numerically studied the kinetic energy release of the photofragments, the angular distribution of the photofragments, as well as the coincident spectra of angular distribution and kinetic energy of the photofragments. Using those observable values, we discuss the features of photodissociation dynamics via resonance or not. It was shown that, in the case of weak UV field, the KER spectra consist of a single resonance, increasing of the field intensity results the appearance of additional spectral structures, due to the involved of higher partial waves through electronic Rabi flopping. The involvement and domination of higher rovibrational states in strong fields result in additional maxima in ADP profile, in addition to the peak at  $\beta = 0$ . The studied coincident KER-ADP spectra clearly represent the correlated dissociation dynamics induced and perturbed by intense UV pulse, the characteristics cannot be observed from separate integrated KER and ADP spectra. The numerical analysis of constructing the ADP profile for a specific energy allows us to get details of rotational wave packet. The present development shows new possibilities for the manipulation of ultrafast photodissociation dynamics in the strong fields.

#### ACKNOWLEDGMENTS

Grants from NSFC (No. 11934004, No. 11974230), the National Basic Research Program of China (2017YFA0403200), the National Key Research and Development Program of China (2020YFA0211300) are acknowledged. V.K. acknowledges financial support from the Swedish Research Council (No. 2019-03470).

- [1] H. Stapelfeldt and T. Seideman, Colloquium: Aligning molecules with strong laser pulses, *Rev. Mod. Phys.* **75**, 543 (2003).
- [2] F. Krausz and M. Ivanov, Attosecond physics, *Rev. Mod. Phys.* **81**, 163 (2009).
- [3] Q. Miao, J.-C. Liu, H. Ågren, J.-E. Rubensson, and F. Gel'mukhanov, Dissociative X-ray Lasing, *Phys. Rev. Lett.* **109**, 233905 (2012).
- [4] B. Rudek, S.-K. Son, L. Foucar, S. W. Epp, B. Erk *et al.*, Ultra-efficient ionization of heavy atoms by intense X-ray free-electron laser pulses, *Nat. Photon.* **6**, 858 (2012).
- [5] P. V. Demekhin and L. S. Cederbaum, Light-induced conical intersections in polyatomic molecules: General theory, strategies of exploitation, and application, *J. Chem. Phys.* **139**, 154314 (2013).
- [6] F. Gel'mukhanov, M. Odelius, S. P. Polyutov, A. Föhlisch, and V. Kimberg, Dynamics of resonant x-ray and Auger scattering, *Rev. Mod. Phys.* **93**, 035001 (2021).
- [7] H. Li, X. Gong, H. Ni, P. Lu, X. Luo *et al.*, Light-induced ultrafast molecular dynamics: From photochemistry to optochemistry, *J. Phys. Chem. Lett.* **13**, 5881 (2022).
- [8] D. Strickland and G. Mourou, Compression of amplified chirped optical pulses, *Opt. Commun.* **56**, 219 (1985).

- [9] C. Spielmann, N. H. Burnett, S. Sartania, R. Koppitsch, M. Schnürer *et al.*, Generation of coherent X-rays in the water window using 5-femtosecond laser pulses, *Science* **278**, 661 (1997).
- [10] P. Emma, R. Akre, J. Arthur, R. Bionta, C. Bostedt *et al.*, First lasing and operation of an Ångström-wavelength free-electron laser, *Nat. Photon.* **4**, 641 (2010).
- [11] K. Zhao, Q. Zhang, M. Chini, Y. Wu, X. Wang *et al.*, Tailoring a 67 attosecond pulse through advantageous phase-mismatch, *Opt. Lett.* **37**, 3891 (2012).
- [12] E. Allaria, R. Appio, L. Badano, W. A. Barletta, S. Bassanese *et al.*, Highly coherent and stable pulses from the FERMI seeded free-electron laser in the extreme ultraviolet, *Nat. Photon.* **6**, 699 (2012).
- [13] M. Harmand, R. Coffee, M. R. Bionta, M. Chollet, D. French *et al.*, Achieving few-femtosecond time-sorting at hard X-ray free-electron lasers, *Nat. Photon.* **7**, 215 (2013).
- [14] C. Pellegrini, A. Marinelli, and S. Reiche, The physics of x-ray free-electron lasers, *Rev. Mod. Phys.* **88**, 015006 (2016).
- [15] C. Bostedt, S. Boutet, D. M. Fritz, Z. Huang, H. J. Lee *et al.*, Linac Coherent Light Source: The first five years, *Rev. Mod. Phys.* **88**, 015007 (2016).
- [16] V. Savchenko, J.-C. Liu, M. Odelius, N. Ignatova, F. Gel'mukhanov *et al.*, Photodissociation of water induced by a long UV pulse and probed by high-energy-resolution x-ray-absorption spectroscopy, *Phys. Rev. A* **104**, 032816 (2021).
- [17] J.-C. Liu, N. Ignatova, V. Kimberg, P. Krasnov, A. Föhlisch *et al.*, Time-resolved study of recoil-induced rotation by X-ray pump - X-ray probe spectroscopy, *Phys. Chem. Chem. Phys.* **24**, 6627 (2022).
- [18] O. Travnikova, E. Kukk, F. Hosseini, S. Granroth, E. Itälä *et al.*, Ultrafast dissociation of ammonia: Auger Doppler effect and redistribution of the internal energy, *Phys. Chem. Chem. Phys.* **24**, 5842 (2022).
- [19] D. Sofikitis, P. Glodic, G. Koumariou, H. Jiang, L. Bougas *et al.*, Highly Nuclear-Spin-Polarized Deuterium Atoms from the UV Photodissociation of Deuterium Iodide, *Phys. Rev. Lett.* **118**, 233401 (2017).
- [20] A. P. O'Connor, A. Becker, K. Blaum, C. Breitenfeldt, S. George *et al.*, Photodissociation of an Internally Cold Beam of  $\text{CH}^+$  Ions in a Cryogenic Storage Ring, *Phys. Rev. Lett.* **116**, 113002 (2016).
- [21] M. McDonald, I. Majewska, C.-H. Lee, S. S. Kondov, B. H. McGuyer *et al.*, Control of Ultracold Photodissociation with Magnetic Fields, *Phys. Rev. Lett.* **120**, 033201 (2018).
- [22] H. B. Pedersen, S. Altevogt, B. Jordon-Thaden, O. Heber, M. L. Rappaport *et al.*, Crossed Beam Photodissociation Imaging of  $\text{HeH}^+$  with Vacuum Ultraviolet Free-Electron Laser Pulses, *Phys. Rev. Lett.* **98**, 223202 (2007).
- [23] X. Gong, W. Jiang, J. Tong, J. Qiang, P. Lu *et al.*, Asymmetric Attosecond Photoionization in Molecular Shape Resonance, *Phys. Rev. X* **12**, 011002 (2022).
- [24] R. González-Férez and C. P. Koch, Enhancing photoassociation rates by nonresonant-light control of shape resonances, *Phys. Rev. A* **86**, 063420 (2012).
- [25] S. Taie, S. Watanabe, T. Ichinose, and Y. Takahashi, Feshbach-Resonance-Enhanced Coherent Atom-Molecule Conversion with Ultranarrow Photoassociation Resonance, *Phys. Rev. Lett.* **116**, 043202 (2016).
- [26] F. Brausse, F. Bach, F. Krečinić, M. J. J. Vrakking, and A. Rouzée, Evolution of a Molecular Shape Resonance Along a Stretching Chemical Bond, *Phys. Rev. Lett.* **125**, 123001 (2020).
- [27] P. M. Kraus, D. Baykusheva, and H. J. Wörner, Two-Pulse Field-Free Orientation Reveals Anisotropy of Molecular Shape Resonance, *Phys. Rev. Lett.* **113**, 023001 (2014).
- [28] Y. R. Liu, Y. Wu, J. G. Wang, O. Vendrell, V. Kimberg, and S. B. Zhang, Electron-rotation coupling in diatomics under strong-field excitation, *Phys. Rev. A* **102**, 033114 (2020).
- [29] Y. R. Liu, Y. Wu, J. G. Wang, O. Vendrell, V. Kimberg, and S. B. Zhang, Photodissociation dynamics of the NH molecule under intense VUV pulses, *Phys. Rev. Res.* **2**, 043348 (2020).
- [30] Y. R. Liu, V. Kimberg, Y. Wu, J. G. Wang, O. Vendrell, and S. B. Zhang, Ultraviolet pump-probe photodissociation spectroscopy of electron-rotation coupling in diatomics, *J. Phys. Chem. Lett.* **12**, 5534 (2021).
- [31] Y. R. Liu, V. Kimberg, Y. Wu, J. G. Wang, O. Vendrell, and S. B. Zhang, Electron-rotation coupling in UV photodissociation of aligned diatomics, *Phys. Rev. Res.* **4**, 013066 (2022).
- [32] Y. P. Zhu, Y. R. Liu, X. Zhao, V. Kimberg, and S. B. Zhang, Core-excited molecules by resonant intense x-ray pulses involving electron-rotation coupling, *Chin. Phys. Lett.* **38**, 053201 (2021).
- [33] G. J. Halász, Á. Vibók, H.-D. Meyer, and L. S. Cederbaum, Effect of light-induced conical intersection on the photodissociation dynamics of the  $D_2^+$  molecule, *J. Phys. Chem. A* **117**, 8528 (2013).
- [34] G. J. Halász, A. Csehi, Á. Vibók, and L. S. Cederbaum, Influence of light-induced conical intersection on the photodissociation dynamics of  $D_2^+$  starting from individual vibrational levels, *J. Phys. Chem. A* **118**, 11908 (2014).
- [35] A. Csehi, G. J. Halász, L. S. Cederbaum, and Á. Vibók, Photodissociation of  $D_2^+$  induced by linearly chirped laser pulses, *J. Chem. Phys.* **143**, 014305 (2015).
- [36] A. Csehi, G. J. Halász, L. S. Cederbaum, and Á. Vibók, Tracking the photodissociation probability of  $D_2^+$  induced by linearly chirped laser pulses, *J. Chem. Phys.* **144**, 074309 (2016).
- [37] A. Tóth, P. Badankó, G. J. Halász, Á. Vibók, and A. Csehi, Importance of the lowest-lying II electronic state in the photodissociation dynamics of LiF, *Chem. Phys.* **515**, 418 (2018).
- [38] A. Tóth, A. Csehi, G. J. Halász, and Á. Vibók, Photodissociation dynamics of the LiF molecule: Two- and three-state descriptions, *Phys. Rev. A* **99**, 043424 (2019).
- [39] X. X. Dong, Y. R. Liu, V. Kimberg, O. Vendrell, Y. Wu, J. G. Wang, J. Chen, and S. B. Zhang, Carrier-envelope-phase measurement of sub-cycle UV pulses using angular photofragment distributions, *Commun. Phys.* **5**, 181 (2022).
- [40] R. Schinke, *Photodissociation Dynamics: Spectroscopy and Fragmentation of Small Polyatomic Molecules* (Cambridge University Press, Cambridge, 1995).
- [41] B. Dutta, R. Bhattacharya, and S. S. Bhattacharyya, Resonance enhancement of two-frequency multiphoton dissociation of  $\text{HD}^+$ , *Phys. Rev. A* **80**, 043413 (2009).
- [42] A. S. Sandhu, E. Gagnon, R. Santra, V. Sharma, W. Li *et al.*, Observing the creation of electronic feshbach resonances in soft X-ray-induced  $\text{O}_2$  dissociation, *Science* **322**, 1081 (2008).
- [43] O. Atabek, R. Lefebvre, C. Lefebvre, and T. T. Nguyen-Dang, Intense-field zero-width resonances and control of molecular photodissociation, *Phys. Rev. A* **77**, 043413 (2008).

- [44] R. Lefebvre, O. Atabek, M. Šindelka, and N. Moiseyev, Resonance Coalescence in Molecular Photodissociation, *Phys. Rev. Lett.* **103**, 123003 (2009).
- [45] P. J. Sarre, C. J. Whitham, and M. M. Graff, An experimental and theoretical study of shape resonances in  $\text{CH}^+$ , *J. Chem. Phys.* **90**, 6061 (1989).
- [46] Z. Biglari, A. Shayesteh, and A. Maghari, Ab initio potential energy curves and transition dipole moments for the low-lying states of  $\text{CH}^+$ , *Comput. Theor. Chem.* **1047**, 22 (2014).
- [47] R. N. Zare, *Angular Momentum: Understanding Spatial Aspects in Chemistry and Physics* (John Wiley & Sons, New York, 1988).
- [48] M. Beck, A. Jäckle, G. Worth, and H.-D. Meyer, The multiconfiguration time-dependent hartree (MCTDH) method: A highly efficient algorithm for propagating wavepackets, *Phys. Rep.* **324**, 1 (2000).
- [49] G. A. Worth, M. H. Beck, A. Jäckle, O. Vendrell, and H.-D. Meyer, The MCTDH Package, Version 8.2, 2000; H.-D. Meyer, Version 8.3, 2002, Version 8.4, 2007; O. Vendrell and H.-D. Meyer Version 8.5, 2013. Version 8.5 contains the ML-MCTDH algorithm. Current versions: 8.4.18 and 8.5.11, 2019. Used version: exchange with Used version. See <http://mctdh.uni-hd.de/>.
- [50] S. B. Zhang and N. Rohringer, Photoemission spectroscopy with high-intensity short-wavelength lasers, *Phys. Rev. A* **89**, 013407 (2014).